Journal of Controlled Release 373 (2024) 481–492

Contents lists available at ScienceDirect

Journal of Controlled Release

journal homepage: www.elsevier.com/locate/jconrel

Biofluid specific protein coronas affect lipid nanoparticle behavior in vitro

Demian van Straten [a,*], Helena Sork [b], Luuk van de Schepop [a], Rowan Frunt [a], Kariem Ezzat [c], Raymond M. Schiffelers [a]

[a] CDL Research, University Medical Center Utrecht, Utrecht, the Netherlands
[b] Institute of Technology, University of Tartu, 50411 Tartu, Estonia
[c] Regain Therapeutics, 141 52 Huddinge, Sweden

ARTICLE INFO

Keywords:
Lipid nanoparticles
Protein corona
Brain
Biofluids
RNA delivery
Characterization

ABSTRACT

Lipid nanoparticles (LNPs) have successfully entered the clinic for the delivery of mRNA- and siRNA-based therapeutics, most recently as vaccines for COVID-19. Nevertheless, there is a lack of understanding regarding their in vivo behavior, in particular cell targeting. Part of this LNP tropism is based on the adherence of endogenous protein to the particle surface. This protein forms a so-called corona that can change, amongst other things, the circulation time, biodistribution and cellular uptake of these particles. The formation of this protein corona, in turn, is dependent on the nanoparticle properties (e.g., size, charge, surface chemistry and hydrophobicity) as well as the biological environment from which it is derived. With the potential of gene therapy to target virtually any disease, administration sites other than intravenous route are considered, resulting in tissue specific protein coronas. For neurological diseases, intracranial administration of LNPs results in a cerebral spinal fluid derived protein corona, possibly changing the properties of the lipid nanoparticle compared to intravenous administration. Here, the differences between plasma and CSF derived protein coronas on a clinically relevant LNP formulation were studied in vitro. Protein analysis showed that LNPs incubated in human CSF (C-LNPs) developed a protein corona composition that differed from that of LNPs incubated in plasma (P-LNPs). Lipoproteins as a whole, but in particular apolipoprotein E, represented a higher percentage of the total protein corona on C-LNPs than on P-LNPs. This resulted in improved cellular uptake of C-LNPs compared to P-LNPs, regardless of cell origin. Importantly, the higher LNP uptake did not directly translate into more efficient cargo delivery, underlining that further assessment of such mechanisms is necessary. These findings show that biofluid specific protein coronas alter LNP functionality, suggesting that the site of administration could affect LNP efficacy in vivo and needs to be considered during the development of the formulation.

1. Introduction

Gene therapy has the potential to treat virtually any disease by means of gene silencing, induction of protein synthesis or gene correction. This potential is held back by delivery related issues. Naked genetic material can evoke host immune responses, is rapidly degraded by endogenous nucleases upon administration and most nucleic acids are unable to escape circulation and enter target cells efficiently without a delivery vehicle [1]. The most advanced delivery option to date are lipid nanoparticles (LNPs) that can encapsulate nucleic acids such as mRNA, siRNA and DNA, protect them from degradation in circulation and facilitate their uptake by cells [2,3]. Onpattro was the first such LNP based siRNA therapy to enter the clinic for the treatment of transthyretin-mediated amyloidosis by predominantly targeting liver hepatocytes [4,5].

Although carefully engineered, it is not the designed synthetic identity of the LNPs that drives their uptake by hepatocytes, but plasma biomolecules that adhere to the particle surface upon administration. This layer of biomolecules that surround the LNP create a new biological identity, a so-called biomolecular corona that includes sugars, lipids and, most importantly, proteins, that ultimately drives the interactions between LNPs and cells [6–8]. For Onpattro, the adsorption of apolipoprotein E (ApoE) to its surface is crucial for its liver tropism [9].

How the LNP protein corona develops, what are its constituents and how it influences LNP behavior has been a topic of many recent investigations and debates [7,10–13]. The formation of a protein corona is a dynamic process and depends on many factors such as nanoparticle shape, size, surface charge, PEGylation, lipid composition etc. [reviewed

* Corresponding author.
E-mail address: d.vanstraten@umcutrecht.nl (D. van Straten).

https://doi.org/10.1016/j.jconrel.2024.07.044
Received 1 November 2023; Received in revised form 16 July 2024; Accepted 17 July 2024
Available online 25 July 2024

by [7,14,15]]. In turn, the composition of the protein corona is crucial for LNP stability [16], biodistribution [17,18], cellular uptake [19] and transfection efficiency [10] and thus LNP functionality. To illustrate, Cheng et al. [17] have shown that by changing the LNP lipid composition, different proteins are attracted to the LNP surface and the tropism of an LNP can be redirected from predominantly targeting the liver to accumulate more in the spleen or lungs, thereby underlining the importance of the protein corona for the intended application of an LNP based therapy.

However, the protein corona composition is not only determined by the physicochemical properties of the nanoparticle. Logically, the corona is also based on the location of nanoparticle administration, as different configurations of biomolecules are present in different tissues and fluids. A variety of protein coronas can therefore be expected on the same particle when administered subcutaneously, intravenously, or intracranially [20–22]. As the potential of gene therapy has drawn the attention of different disciplines within the drug development, more of these administration routes will be explored. For instance, many neurological diseases lack therapeutic options due to the complexity of central nervous system (CNS) disorders, the fragility and limited regenerative capacity of neurological tissues and physical barriers that prevent efficient drug delivery [23,24]. Gene therapy provides an interesting approach for several of these complex diseases, especially with the development of non-viral vectors such as LNPs [23,25]. However, the usual intravenous administration of LNPs is not feasible for central nervous system applications due to the presence of the blood brain barrier (BBB), which prevents the nanoparticles from entering the brain efficiently. Intracranial administration could therefore be considered, resulting in a cerebrospinal fluid (CSF) based protein corona as opposed to a plasma protein corona after intravenous injection, possibly altering the behavior of the LNP. It has been observed that gold nanoparticles develop a different corona after traversing through an in vitro BBB model, indicating different coronas do indeed develop in different biological compartments, which could affect LNP functionality [26]. Yet, little is known about the LNP protein corona formation in CSF and its consequences on LNP efficacy.

Here, the Onpattro LNP formulation was used to compare the protein corona formed after incubating the particles in CSF or plasma of human origin. The protein corona composition, cellular uptake, and cargo delivery efficiency of LNPs were investigated in vitro, to determine the differences between intravenous and intracranial administration. This will give insight on the intricacies of using local delivery of LNPs for neurological diseases.

2. Materials and methods

2.1. Buffers, reagents, materials

Phosphate buffered saline (PBS), dexamethasone, bovine serum albumin (BSA), distearoylphosphatidylcholine (DSPC) and cholesterol were purchased from Sigma-Aldrich (NL). DLin-MC3-DMA was obtained from GKV Bio. 1,2-Dimyristoyl-rac-glycero-3-methoxypolyethylene glycol-2000 (DMG-PEG(2000)) and 1,2-distearoyl-sn-glycero-3-phosphoethanolamine-N-[biotinyl(polyethylene glycol)-2000] (DSPE-PEG (2000)-biotin) (Avanti Polar Lipids, Alabama, USA). Lipofectamine RNAiMAX (Invitrogen, NL). Anti-Firefly siRNA molecules were obtained from Integrated DNA Technologies (Iowa, USA). Single stranded molecules were annealed in-house for 5 min at 97 °C. siRNA sequence: Sense: '5-GGA CGA GGU GCC UAA AGG AdCdG-3' Antisense: '5-UCC UUU AGG CAC CUC GUC CdCdG-3'.

2.2. LNP production

LNPs were prepared via microfluidic mixing using a Nanoassemblr Benchtop device (Precision Nanosystems, Canada). In short, DLin-MC3-DMA, Cholesterol, DSPC, DMG-PEG(2000), and DSPE-PEG(2000)-biotin were dissolved in an ethanol phase. A molar ratio of 50: 38.5: 10: 1.5 and 50: 38.5: 9: 1.5: 1 was used for control and biotinylated LNPs respectively, to a final lipid concentration of 10 mM. For the aqueous phase, an acetate buffer (25 mM, pH 4.0) was prepared with a final siRNA concentration of 2.5 μM. The Nanoassemblr was set to a flowrate of 4 mL/min and a flow rate ratio of 3:1 (aqueous to solvent phase) to mix the phases. The obtained LNP suspension (N/P of 6) was dialyzed against PBS overnight using a Slide-A-Lyzer, 20 k molecular weight cut-off (MWCO) dialysis cassette (Thermo Scientific, Massachusetts, USA) in the dark at 4 °C. The final product was stored at 4 °C in the dark.

The mean *Z*-average particle size of LNPs was determined via dynamic light scattering (DLS). Micelle stocks were diluted 1:20 in PBS and analyzed at 25 °C using a ZetaSizer Nano ZS 90 (Malvern Analytical, UK).

To determine the successful decoration of the LNP surface with biotin groups, the capture of fluorescently labeled biotinylated and non-biotinylated LNPs by streptavidin coated beads was compared. Streptavidin coated magnetic beads (Dynabeads MyOne Streptavidin C1, Fischer Scientific, NL) were incubated with the LNPs in PBS for 2 h at RT. The beads were subsequently washed several times with PBS and the mean fluorescence intensity (MFI) was quantified using a BD FACSCanto II (BD Biosciences, New Jersey, USA). For the binding competition experiment, increasing amounts of non-fluorescent biotinylated LNPs were added to a fixed amount of fluorescently labeled biotin-LNPs and subjected to the same incubation, capture and FACS protocol as described above.

2.3. Biofluid protein corona formation

To investigate protein corona formation on LNPs in different biological fluids, biotinylated LNPs were incubated in CSF or plasma and subsequently isolated via a combination of methods. First, human plasma and CSF were normalized to 5 mg/mL total protein concentration. For plasma, the protein concentration was determined via a Micro BCA Protein kit (Thermo Scientific, NL) and subsequently diluted accordingly with PBS.

Due to its low inherent protein content, CSF needed to be concentrated using centrifugal ultrafiltration using a 3 k MWCO filter (VIVASPIN 20, VWR International, USA). The protein concentration was determined by microBCA and adjusted with PBS when necessary. Biotinylated LNPs were diluted (1:5 *v*/v) in the biological fluid of interest and incubated for 1 h at 37 °C under agitation, to allow LNP protein corona formation.

Afterwards, LNPs were separated from bulk free protein via size exclusion chromatography (SEC) with an ÄKTA™ start protein purification system (Cytiva, NL) equipped with two HiScreen Capto Core 700 columns (Cytiva, NL) coupled in series and a Frac30 round fraction collector (GE Healthcare, NL). This system allows separation based on size exclusion and affinity based binding chromatography. LNP containing fractions were identified based on size of the particles (UV/vis detection on the ÄKTA) together with the fluorescence of the LNP containing fractions as measured with a Spectramax iD3 plate reader (Molecular Devices, California, USA). For control samples, PBS was added to CSF and plasma instead of LNP suspensions and subsequently subjected to the same separation protocol and the same fractions were collected for further analysis.

2.4. Silver staining

The protein content of a dilution range of CSF and plasma was separated via gel electrophoresis and visualized via silver staining. To this end, CSF and plasma protein concentration were normalized to 5 mg/mL as described previously and further diluted using PBS to achieve the desired concentrations. The fluids were subsequently mixed 2:1 with 3× Laemmli buffer (150 mM Tris-HCl (pH 6.8), 6% SDS, 0.3% Bromophenol blue, 30% *v*/v Glycerol) with 25 mM DTT and heated for 10 min

at 95 °C. The samples were loaded in a Bolt 4–12% bis-tris 10-well gel in MES SDS buffer (Invitrogen, NL) and separated at 165 V for 35 min. The gel was stained using a Pierce silver stain kit (Thermo Scientific, NL) according to manufacturer's instructions.

For protein corona analysis, LNPs were incubated in the biological fluids and isolated via SEC as described previously. Pooled LNP containing SEC fractions were incubated with a high-capacity streptavidin agarose resin (Thermo Scientific, NL) to isolate LNPs via immunoprecipitation. Corresponding control fractions were also pooled and subjected to the same procedure to account for aspecific protein binding to the resin. Per sample, 50 μL resin (prewashed with PBS) was added and incubated overnight at 4 °C under light agitation. The resin was isolated via centrifugation and washed with three times PBS to remove unbound protein. Resin bound LNPs and protein were removed by adding RIPA buffer (with protease inhibitor, Merck, Germany) and incubating on ice for 1 h. The resin was pelleted and 40 μL supernatant was collected and processed for gel electrophoresis and silver staining as described above.

2.5. Cell culture

U87-MG and MDA-MB-231 were cultured in DMEM supplemented with 10% FCS (Gibco, Massachusetts, USA) and 1% penicillin-streptomycin (PS) (Fisher Scientific, New Hampshire, USA). HMEC-1 were cultured on 0.1% gelatin coated plates in MCDB-131 medium supplemented with 10% FBS (Gibco, Massachusetts, USA), 2 × 10–3 M L-glutamine (Gibco, Massachusetts, USA), 10 ng mL − 1 rhEGF (Peprotech, Korea), and 50 × 10–9 M hydrocortisone (Sigma-Aldrich, NL). The brain endothelial cell line hCMEC/D3 (kindly gifted by M. Fens) was cultured on 10 μg/mL rat tail collagen (Corning, New York, USA) coated plates in EBM-2 (Promocell, Germany) supplemented with hydrocortisone, hFGF-B, VEGF (Vascular Endothelial Growth Factor), R3-IGF-1, ascorbic acid, hEGF, GA-1000 and 1% FBS (derived from the EGM-2 SingleQuots bullet kit, Lonza, Switzerland). Cells were kept at 37 °C and 5% CO_2.

A dual luciferase expression system was used to investigate functional siRNA delivery by LNPs. All cell lines were genetically modified to stably express two luciferase proteins as described by Evers et al. [27]. In short, cell lines were transfected with a pHAGE2-PGK-FFluc-SV40-Rluc-NeoR_fusion-WPRE construct to stably express both Firefly and *Renilla* luciferase. A G418-resistance was introduced, and cells were cultured with 500–1000 μg mL − 1 G418 to maintain plasmid expression. Cell lines expressing this system are referred to as *-dluc (*e.g., U87-*dluc*).

2.6. LNP uptake

For uptake experiments, cells were seeded (1.5 × 10^4 cells/well for HMEC and HCMEC and 1.2 × 10^4 cells/well for U87 and MDA-MB-231) in a 48-well plate (plates were pre-coated with gelatin or collagen for HMEC and HCMEC respectively). After cells were allowed to adhere overnight, they were washed with serum/additives free media to remove any interfering protein from the standard culture conditions. Fresh media were generated containing 10% PBS, CSF, plasma, or FCS (5 mg/mL starting protein concentration) and 1% PS and sterile filtered using a 0.45 μm PVDF filter. Fluorescently labeled LNPs were added to the uptake sera to a final concentration of 10 nM total siRNA (2.5 nM fluorescently labeled siRNA) and sterile filtered using a 0.45 μm PVDF filter. Per well, a medium/LNP suspension of 1.5 pMol total siRNA was added and incubated for 4, 24 and 48 h. After incubation, cells were washed with serum free medium and subsequently detached with trypsin (Gibco, Massachusetts, USA) and collected. Trypsin was inactivated by addition of trypsin neutralizing solution (Sigma-Aldrich, NL). Cells were spun down 5 min 300 xg to remove trypsin and washed with cold PBS. Cells were then resuspended in PBS + 1% BSA (PBA) and their fluorescence measured using a BD FACS Canto II (BD Biosciences, NL). Cell mean fluorescence intensity (MFI) was analyzed with FACS Diva software.

2.7. Knockdown

For knockdown experiments, dual luciferase expressing cells were seeded at 5 × 10^3 cells/well in a 96-well plate (plates were pre-coated with gelatin or collagen for HMEC and HCMEC respectively). After cells were allowed to adhere overnight, they were washed with their respective serum/additives free media to remove any interfering protein from the standard culture conditions. Fresh media were generated with 10% PBS, CSF, plasma, or FCS (5 mg/mL starting protein concentration) and 1% PS and sterile filtered using a 0.45 μm PVDF filter. Fluorescently labeled LNPs were added to the uptake sera to a final concentration of 10 nM anti-firefly luciferase siRNA and sterile filtered using a 0.45 μm PVDF filter. Per well a total of 1pMol siRNA was added and incubated for 24 and 48 h. RNAiMAX was used according to manufacturer's protocol as a positive control for siRNA mediated knockdown. After the respective incubation times, luciferase activity was measured via the Dual-Luciferase reporter system kit (Promega, NL) according to manufacturer's instructions. Luminescence was measured using a Spectramax iD3 plate reader (Molecular Devices, USA). A ratio of both luciferase activities was used as a read out for LNP mediated knockdown.

2.8. APOE detection in protein corona

CSF and plasma protein concentrations were normalized to 5 mg/mL. In a 96-well plate, 150 μL/well biofluid was added. To each well, 10 μL fluorescent LNP suspension was added and incubated for 1 h at 37 °C under light agitation. After protein corona formation, LNPs were isolated via bead mediated immunoprecipitation using C1 Streptavidin beads (Thermo Scientific, NL). In short, beads were prewashed three times with PBS. After resuspending the beads in PBS, 3 μg beads was added per well and incubated at room temperature for 1 h under agitation. Beads were subsequently isolated from their media by magnetic separation and washed twice with PBA. After resuspension in PBA the beads were incubated with anti-human ApoE antibody (Biotechne, US) for 1 h at RT. Beads were washed twice with PBA and incubated with goat anti-mouse Alexa Fluor 488 (Thermo Fischer, NL) for 30 min at RT in the dark. Subsequently, beads were washed twice with PBA and their fluorescence was measured using a BD FACS Canto II (BD Biosciences, New Jersey, USA). The bead MFI was analyzed with FACS Diva software.

2.9. Sample preparation for nano-LC-MS/MS

Sample volume was reduced with 10 kDa MWCO filters and then proteins were precipitated (15 μg) with the trichloroacetic acid deoxycholate (TCA/DOC) method, as described elsewhere (Joint ProteomicS Laboratory (JPSL) of the Ludwig Institute for Cancer Research; Walter and Eliza Hall Institute of Medical Research, 2006). Protein pellets were suspended in 7 M urea / 2 M thiourea, 100 mM ammonium bicarbonate (ABC), 20 mM methylamine solution, followed by disulfide reduction and cysteine alkylation with 5 mM DTT and 10 mM chloroacetamide for 60 min, each at room temperature. Proteins were predigested with 1:50 (enzyme to protein) Lys-C (Wako Chemicals) for 4 h, diluted 5 times with 100 mM ABC and further digested with trypsin (Sigma-Aldrich, NL) overnight at room temperature. Peptides were desalted with in-house made C18 StageTips.

2.10. Nano-LC-MS/MS measurement

Samples were injected to an Ultimate 3000 RSLCnano system (Dionex, California, USA) using a C18 trap-column (Dionex, California, USA) and an in-house packed (3 μm C18 particles, Dr. Maisch, Germany) analytical 50 cm × 75 μm ID emitter-column (New Objective, Massachusetts, USA). Peptides were eluted at 200 nL/min with an 8–40% B 120 min gradient (buffer B: 80% acetonitrile +0.1% formic acid, buffer A: 0.1% formic acid) to a Q Exactive HF (Thermo Fisher Scientific, Massachusetts, USA) mass spectrometer (MS) using a nano-electrospray

source (spray voltage of 2.5 kV). The MS was operated with a top-12 data-dependent acquisition strategy. Briefly, one 350–1400 *m/z* MS scan at a resolution setting of $R = 60{,}000$ at 200 m/z was followed by higher-energy collisional dissociation fragmentation (normalized collision energy of 26) of 12 most intense ions (z: +2 to +6) at $R = 30{,}000$. MS and MS/MS ion target values were 3e6 and 1e5 with 50 and 45 ms injection times. Dynamic exclusion was limited to 40 s.

2.11. Nano-LC-MS/MS raw data processing

Mass spectrometric raw files were analyzed with the MaxQuant software (version 2.0.3.0) (Cox & Mann, 2008). Methionine oxidation, asparagine, and glutamine deamidation and protein N-terminal acetylation were set as variable modifications, while cysteine carbamidomethylation was defined as a fixed modification. Search was performed against UniProt (www.uniprot.org) *Homo sapiens* reference proteome database (downloaded on 20.09.2020) using the tryptic digestion rule (including cleavages after proline). Only identifications with minimally 1 peptide 7 amino acids long were accepted and transfer of identifications between runs was enabled. Label-free normalization with MaxQuant LFQ algorithm was also applied. Protein and LFQ ratio count (i.e., number of quantified peptides for reporting a protein intensity) was set to 1. Peptide-spectrum match and protein false discovery rate (FDR) was kept below 1% using a target-decoy approach. All other parameters were default.

3. Results

3.1. Biotinylation allows isolation of LNPs from biological matrices

To investigate the protein corona formation in different biological fluids, LNPs were incubated in human plasma (P-LNPs) or human CSF (C-LNPs) and subsequently isolated to study the surface bound proteins (Fig. 1). Here, a multimodal chromatography approach was used to separate LNPs from bulk protein, followed by affinity-based isolation, depending on the subsequent method of analysis (Fig. 1).

DSPE-PEG(2000)-biotin was incorporated in the Onpattro formulation to facilitate biotin-streptavidin based isolation. The size of the biotinylated LNPs was measured by DLS to be 75 +/− 5 nm which is in line with what is reported in literature for similar formulations [9,28]. By incorporating fluorescently labeled siRNA, the LNPs could be visualized and tracked during isolation. Capture of biotinylated fluorescent LNPs by streptavidin beads was observed via flow cytometry whilst negligible capture was seen after incubation with non-biotinylated fluorescent LNPs (Fig. 2A), indicating successful incorporation of DSPE-PEG(2000)-biotin to the LNP surface. Furthermore, a dose dependent decrease of fluorescence was seen on the beads after addition of increasing amounts of non-fluorescent biotinylated LNPs to a fixed amount of fluorescent biotin-LNPs, which shows competition for binding and thus capture specificity (Fig. 2B).

3.2. LNPs develop biofluid specific protein coronas

The biotinylated LNPs were incubated in different biological fluids to allow protein corona formation. To negate the significant inherent difference in protein concentration, both fluids were normalized to 5 mg/mL total protein. After incubation of LNPs in CSF or plasma, LNPs were separated from their biological matrix by chromatographic isolation based on size, charge and hydrophobicity. The presence of LNPs could be confirmed by measuring the fluorescence of fractions after separation (Fig. 3A). The fluorescence was highest in fractions 4–7. This

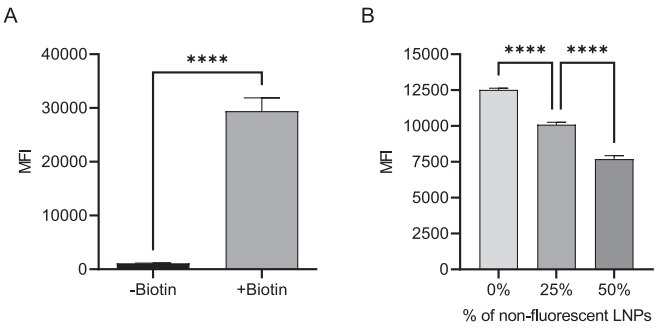

Fig. 2. Incorporation of biotinylated lipids in the LNPs allows capture by streptavidin decorated beads. Biotinylated LNPs (+biotin) bind to streptavidin coated magnetic beads while undecorated LNPs (−biotin) do not, as indicated by the difference in mean fluorescence itensity (MFI) (unpaired *t*-test, $p < 0.0001$) (A). A dose dependent competition for streptavidin moieties is seen after addition of increasing amounts of non-fluorescent biotinylated LNPs to a fixed amount of fluorescent biotinylated LNPs (two-way ANOVA with Tukey's post-hoc, $p < 0.0001$) (B).

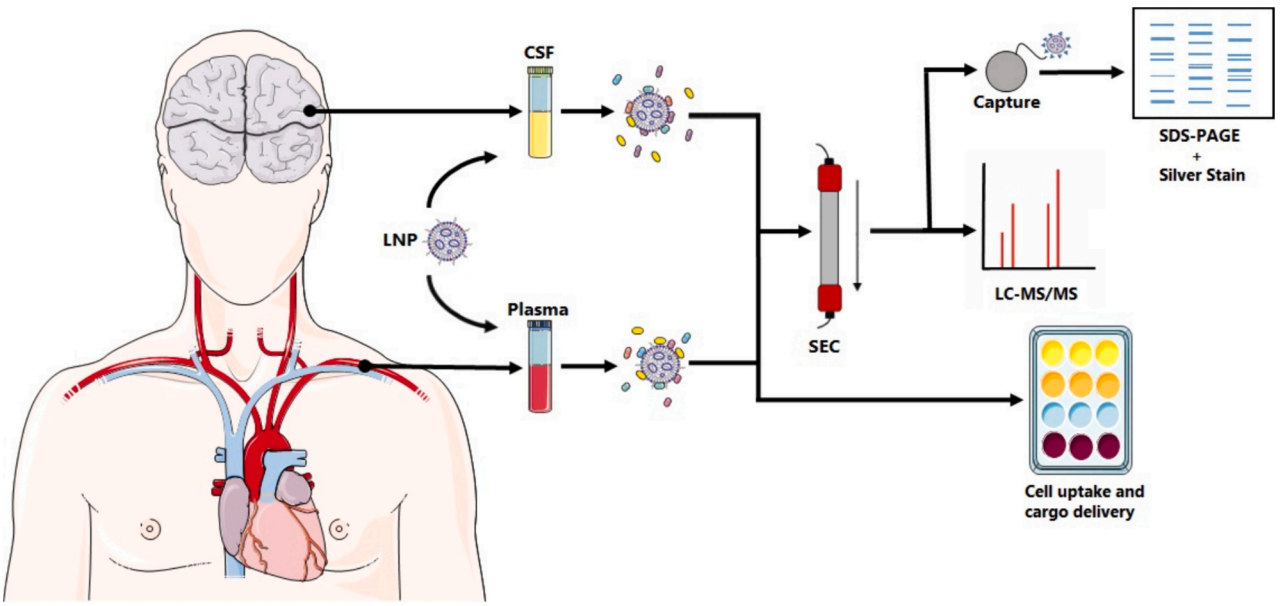

Fig. 1. Schematic representation of the protein corona formation, isolation and characterization protocol.

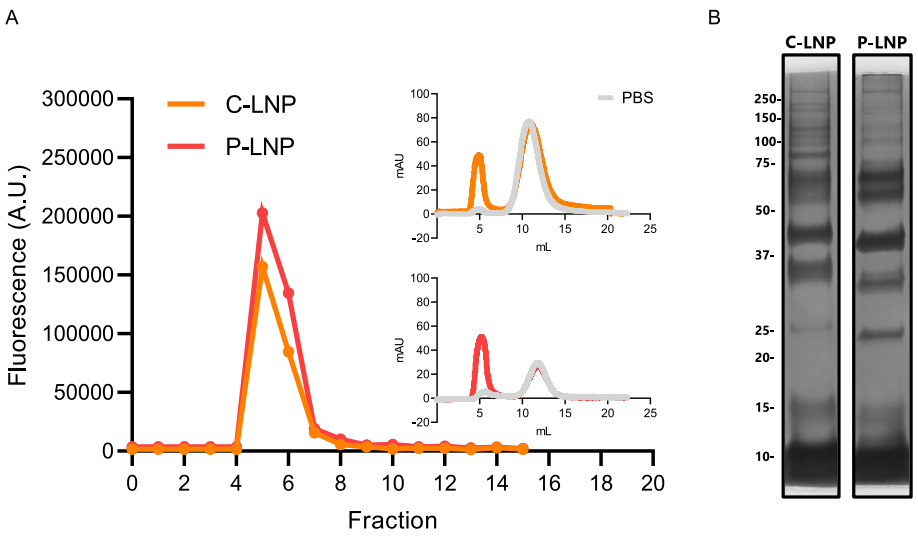

Fig. 3. Multimodal chromatographic separation allows isolation of LNPs from free protein after incubation in plasma or CSF. The fluorescence of fractions collected after SEC, with the LNP containing fractions showing increased fluorescence (main graph). Size exclusion chromatographs of CSF (top insert) and plasma (bottom insert) supplemented with LNPs (colored) or PBS (grey). Silver staining of the protein corona on C-LNPs and P-LNPs (B).

corresponded to the chromatographs where the larger particles eluded first, followed by the more prominent free protein peak. The clear increase of the first peak of larger particles is seen when the fluids contained LNPs compared to the negative control fluids containing PBS, as seen in both CSF (top insert) and plasma (bottom insert).

The LNPs were subsequently extracted from the SEC fractions by streptavidin mediated capture to remove any residual co-eluted natural nanoparticles or free protein. The LNP bound proteins were then separated and stained to generate protein fingerprints used to detect differences in the protein corona on C-LNPs and P-LNPs. A dilution series of CSF and plasma shows different protein patterns between the fluids, confirming that the difference in proteome can be visualized by this technique, even with the normalized protein concentration (Fig. S1). Although similar protein patterns were observed for C-LNP and P-LNP coronas, variations in band intensity are detected as well as several unique proteins per biofluid, indicating subtle differences in protein

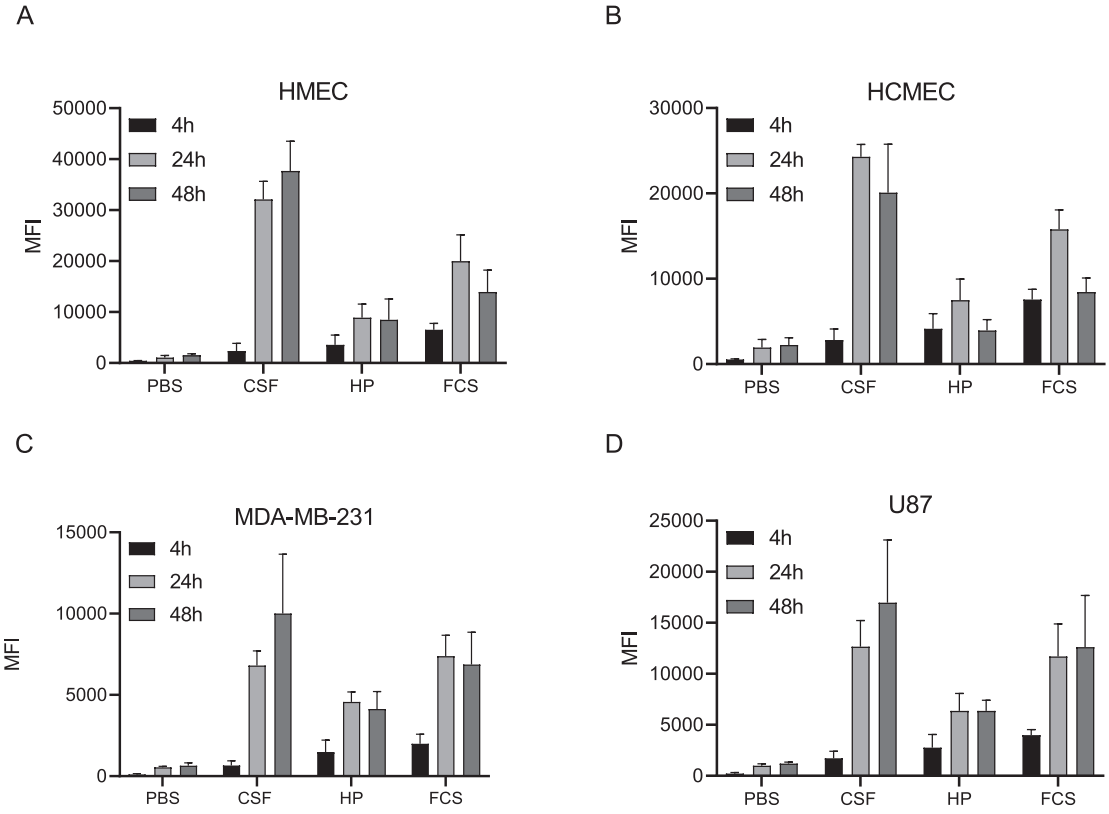

Fig. 4. The uptake of fluorescent LNPs differs between various cell lines in different biological fluids over time. Uptake of LNPs in media supplemented with PBS, CSF, human plasma (HP) or FCS over time by HMEC (A), HCMEC (B), MDA-MB-231 (C) and U87 (D) based on fluorescence as measured by flow cytometry. Statistical significance ($p < 0.05$) was calculated using a two-way ANOVA followed by Tukey's post-hoc and is displayed in Fig. S2.

corona composition (Fig. 3B). For instance, at ~34 kDa a protein band is seen in the P-LNP sample which is slightly shifted upwards in the C-LNP sample. Between 50 kDa and 75 kDa, the P-LNP sample shows two separate bands which are not as clear as in the C-LNP sample. Moreover, a different pattern of protein bands is seen >75 kDa between P-LNP and C-LNP.

3.3. The composition of the protein corona alters the uptake of LNP by cells over time

The effect of the different protein coronas on LNP-cell interactions were investigated. LNPs were presented to brain and peripheral (non-brain) endothelial and tumor cells, in CSF or plasma supplemented medium. Medium supplemented with PBS served as a no-protein control while FCS represented a "traditional" protein composition, generally found in cell culture experiments. LNP uptake was quantified after 4 h, 24 h and 48 h and is depicted in Fig. 4. Heatmaps of the *p*-values describing statistically significant differences between groups are shown in Fig. S2. After 4 h, the peripheral endothelial cell line (HMEC-1) showed the highest uptake of LNPs incubated in FCS, followed by plasma and CSF and lastly PBS. In time, this pattern changed significantly as at 24 h the highest uptake was seen in CSF, followed by FCS, plasma, and PBS, which remained the same after 48 h (Fig. 4A). A similar pattern was seen for brain endothelial cell line HCMEC, while for breast cancer cell line MDA-MB-231 and brain tumor cell line U87, CSF showed a similar uptake to FCS at 24 h and the highest uptake at 48 h (Fig. 4B, C, D). Surprisingly, LNPs were taken up as much or more in CSF compared to all other conditions from 24 h onwards, while at 4 h it was the biological fluid with the least LNP uptake across cell types.

No clear cell type specific interaction was seen for cells with a matching biological matrix (e.g., brain cells with a CSF protein environment). All cell types had the same uptake patterns when comparing the different fluids.

Interestingly, overall uptake did not always increase with time. For HMEC, the highest uptake was seen at 48 h in CSF, but at 24 h for FCS and no difference between 24 h and 48 h in plasma (Fig. 4A). MDA-MB-231 had a similar uptake pattern in time to HMEC, with the highest uptake at 48 h in CSF but no difference between 24 h and 48 h in plasma and FCS (Fig. 4C). HCMEC showed the highest uptake at 24 h for CSF, plasma, and FCS (Fig. 4B). U87 also showed the highest uptake at 48 h in CSF, with no difference between 24 h and 48 h for plasma and FCS (Fig. 4D).

3.4. LNPs acquire relatively more ApoE in CSF than in plasma

The uptake of Onpattro by cells is predominantly mediated by ApoE bound to the LNP surface [9]. Therefore, a comparison was made for the amount of ApoE bound to C-LNPs and P-LNPs via flow cytometry. After bead capture, a higher signal of fluorescent siRNA was measured on P-LNPs compared to C-LNPs, indicating more P-LNPs were captured per bead (Fig. 5A). Surprisingly, non-biotinylated LNPs still bound to the streptavidin beads in plasma, but not in CSF (data not shown). P-LNPs showed a higher absolute value of ApoE3 associated fluorescence compared to C-LNPs (Fig. 5B). Aspecific binding of primary (no LNP) and secondary antibodies was absent. When normalizing the amount of ApoE3 fluorescence to the amount of siRNA fluorescence per bead, more ApoE3 was found per C-LNP compared to P-LNPs based on siRNA fluorescence (Fig. 5C).

3.5. LNP uptake is not a predictor of siRNA target knockdown

The siRNA delivery efficacy of C-LNPs and P-LNPs was compared based on target knockdown. All cell lines used in these experiments were transfected to express both *Renilla* and firefly luciferase to determine the functional delivery of siRNA by LNPs in different biological media. The anti-firefly luciferase siRNA encapsulated in the LNPs does not affect the expression of *Renilla* luciferase. This way the *Renilla* luciferase acts as an internal control to correct for any nonspecific effect on firefly luciferase expression by external factors. Henceforth, luciferase activity will refer to firefly luciferase activity normalized against *Renilla* luciferase activity.

The commercial transfection reagent RNAiMAX showed effective knockdown of firefly luciferase activity in all cell lines indicating that the siRNA molecule is capable of inhibiting expression (Fig. 6). For the LNPs, minor knockdown was observed in the PBS condition in all cell lines at 24 h, although significant knockdown occurred after 48 h in HMEC-*dluc*, HCMEC-*dluc* and MDA-MB-231-*dluc* (Fig. 6A, B & C). The least luciferase activity after 24 h was seen in FCS media in HMEC-*dluc* and HCMEC-*dluc*, indicating the most efficient cargo delivery occurred in this fluid. No difference in luciferase activity was observed in HMEC-*dluc* exposed to LNPs in CSF compared to plasma, while for HCMEC-*dluc* the LNPs performed better in plasma than in CSF. More luciferase activity was observed in PBS than in all other conditions in MDA-MB-231-*dluc* at 24 h. For U87-*dluc*, RNAiMAX showed significant knockdown at 24 h and almost complete knockdown at 48 h. However, reduced luciferase expression was only measured in FCS compared to PBS. All other conditions produced no difference in activity in U87-*dluc* (Fig. 6D).

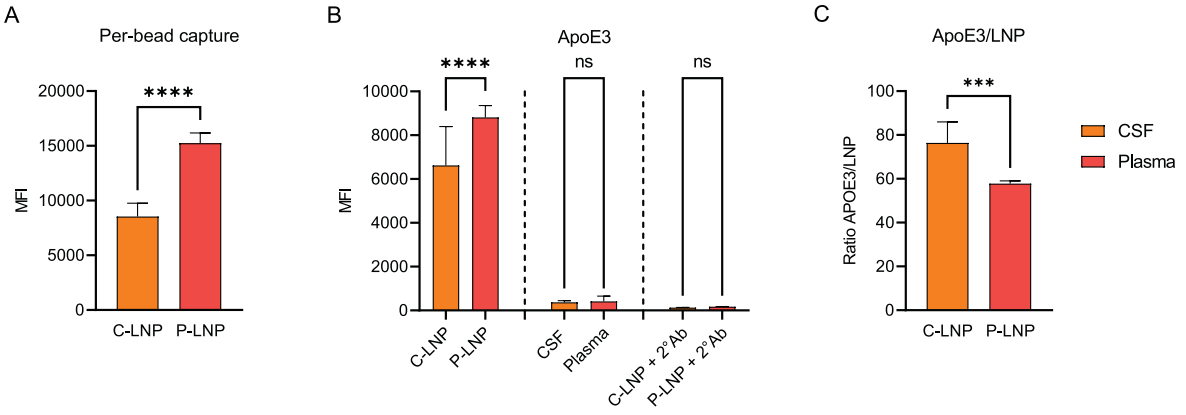

Fig. 5. Detection of APOE on LNPs incubated in CSF and plasma. MFI (mean fluorescence intesity) of streptavidin captured C-LNPs or P-LNPs, reflecting the per-bead capture (paired *t*-test, $p < 0.0001$) (A). Detection of ApoE3 on biotinylated LNPs after incubation in CSF and plasma and subsequent bead capture (two-way ANOVA with Tukey's post-hoc, $p < 0.0001$) (B). Relative amount of ApoE3 detected per LNP based on the fluorescent ratio of siRNA and ApoE (ApoE3/LNP) (paired t-test, $p = 0.0003$) (C).

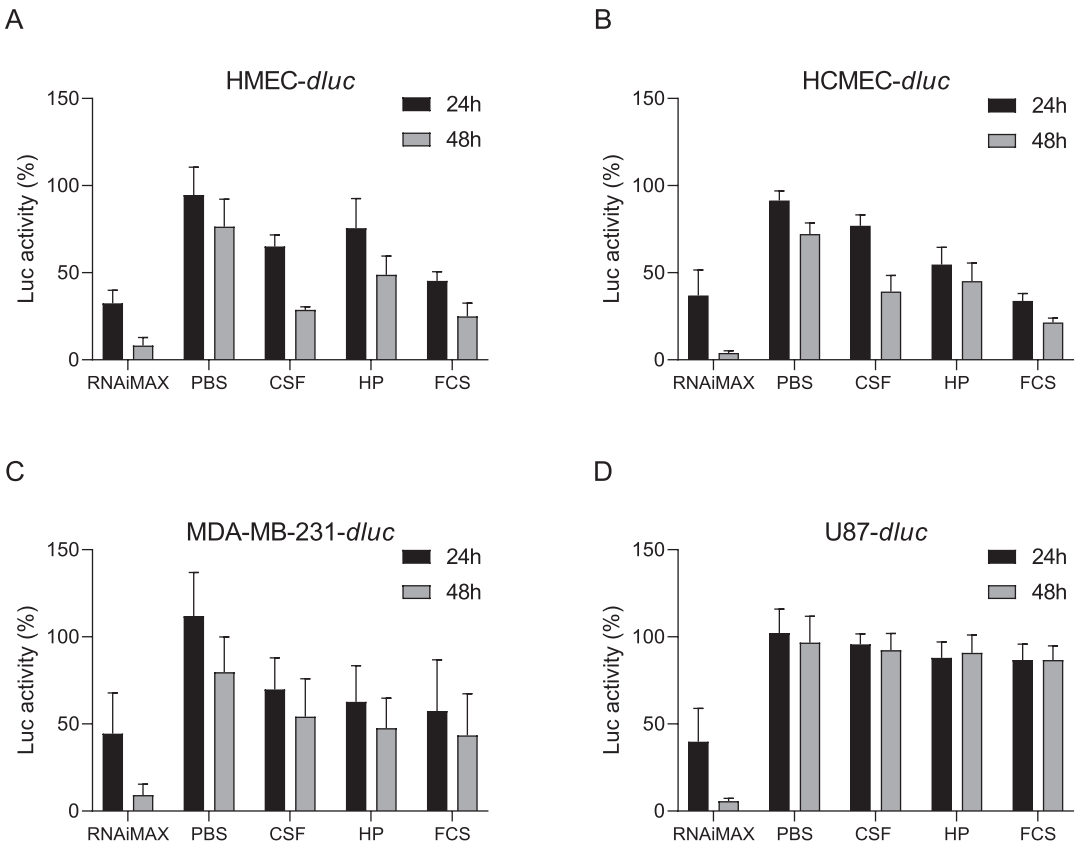

Fig. 6. The cargo delivery efficiency of LNPs differs between various cell lines in different biological fluids over time. Knockdown of firefly luciferase activity in HMEC-*dluc* (A), HCMEC-*dluc* (B), MDA-MB-231-*dluc* (C) and U87-*dluc* (D) after incubation with anti-firefly luciferase LNPs in media supplemented with PBS, CSF, human plasma (HP) or FCS over time. Statistical significance ($p < 0.05$) was calculated using a two-way ANOVA followed by Tukey's post-hoc and is displayed in Fig. S3.

After 48 h, the most efficient knockdown was achieved in FCS and CSF for HMEC-*dluc*, followed by plasma and finally PBS (Fig. 6A). For HCMEC-*dluc*, FCS had the lowest luciferase activity after 48 h, despite more LNPs being taken up in CSF at that timepoint (Fig. 6B and 4B). The second lowest luciferase activity was seen in CSF, followed by plasma, inverse of what was seen at 24 h for this cell line. MDA-MB-231-*dluc* showed a trend with the lowest luciferase activity in FCS, followed by plasma, CSF, and PBS respectively for all time points. Nevertheless, the differences were not significant, except for RNAiMAX and PBS (Fig. 6C). In general, U87-*dluc* was not susceptible for LNP mediated siRNA knockdown (Fig. 6D) and nearly no effect was seen in either condition despite the particles being taken up by the cells (Fig. 4D) and efficacy of the siRNA in the positive controls (Fig. 6D). Heatmaps of the *p*-values of the differences in knockdown between conditions are depicted in Fig. S3.

3.6. C-LNPs and P-LNPs develop different apolipoprotein profiles

To get more detailed information regarding the composition of the different coronas, LNP bound proteins were analyzed via mass spectrometry. The proteins in LNP containing SEC fractions were compared to the same fractions derived from biofluids without LNPs to account for co-isolated proteins in these fractions (Fig. 1). Over all four samples a total of 510 protein hits were included in the abundance calculations, representing 183 unique proteins. The CSF control contained 113 proteins. The C-LNP fractions contained 160 proteins, of which 64 were not found in the CSF control sample. In the plasma control sample, 89 proteins were found. For P-LNPs, 148 proteins were identified of which 75 were not found in the control sample (Fig. S4).

Overall, the corona of C-LNPs was more diverse than P-LNPs with 17 proteins making up 75% of the total protein corona, while for P-LNPs 8 proteins represented 75% of bulk protein (Fig. 7A & Table S1). Remarkably, 5 apolipoproteins as well as other lipid binding proteins were found in LNP samples that were absent when no LNPs were present. In line with previous observations in this study, ApoE made up a larger percentage of the total protein corona on C-LNPs (0.74%) than of the P-LNP corona (0.13%) (Fig. 7B).

Though the repertoire of apolipoproteins was comparable between P-LNPs and C-LNPs (7 vs 8 respectively), the apolipoproteins represented a larger percentage of the total protein on C-LNPs (3.25% vs 1.51%). The top three most abundant lipoproteins for C-LNPs were ApoJ (Clusterin), ApoD and ApoE, while for P-LNPs these were ApoC-III, ApoA-IV and ApoD. Furthermore, >30 immunoglobulin proteins were found that were nearly exclusively identified in LNP containing samples. Interestingly, of the 19 brain specific proteins (exclusively found in CSF), 8 were enriched in C-LNP fractions, adding to the unique protein corona for C-LNPs compared to P-LNPs (Table S1).

4. Discussion

There is a gradually increasing implementation of nanotechnology-based therapies in the clinic [29] and more attention is drawn to the complex interactions between nanoparticles and biological systems, with particular interest in the protein corona. The composition of the protein corona is affected by the site of administration and as most nanoparticles are administered intravenously, the majority of protein corona research is performed in blood, plasma, or serum. However, given the versatility of nucleic acid therapeutics, many targets and

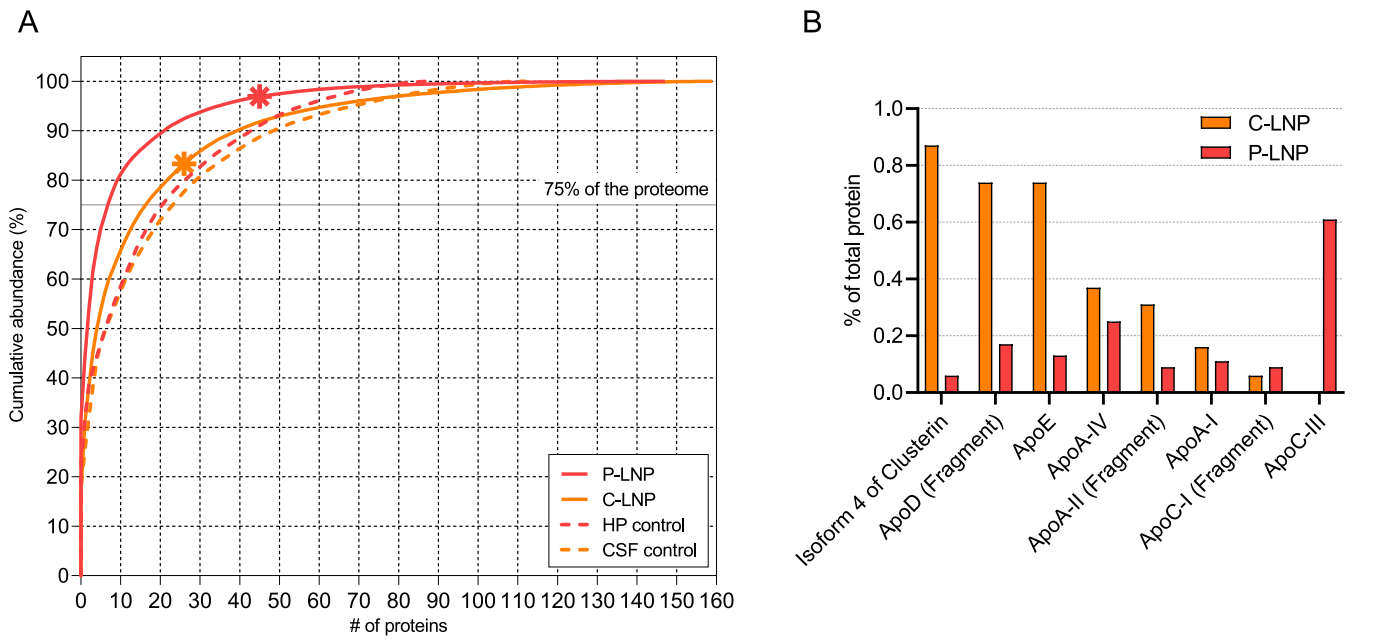

Fig. 7. ApoE represents a higher percentage of total protein in CSF compared to plasma derived coronas. Cumulative abundance of proteins detected by LC-MS/MS on C-LNP, P-LNP and their respective control samples. The asterisks represent ApoE (A). Apolipoproteins represent 3.25% of the total protein corona on C-LNPs and 1.51% of the P-LNP corona (B).

tissues are likely to be explored soon and thus many new biological environments need to be considered during LNP development, such as the CSF for intracranial gene therapy.

To date, little is known about the CSF based protein corona and how it affects LNP functionality. It was observed that the protein corona on gold nanoparticles changes during their journey across the BBB [26] and that carbon nanotubes have a different protein corona after incubation in plasma compared to CSF [22]. It is important to know whether this holds true for LNPs, what the differences in protein content are and whether they affect LNP-cell interactions and cargo delivery. Such information can aid the development of specialized LNP formulations for specific diseases in their respective site of action. To this end, LNPs were incubated in plasma and CSF to characterize the acquired protein coronas and investigate the effects of these coronas on LNP interactions with brain and non-brain cell lines.

It was decided to normalize the protein concentration between the biofluids during experiments. The average protein concentration of human plasma can be over 100-fold higher than that of human CSF [30], which can affect PEG-shedding kinetics [31] and influence protein corona development as well as LNP uptake by cells. Protein concentration normalization ensures that differences in protein corona functionality are based on intrinsic protein properties rather than absolute concentration. Although some note that the protein concentration of the incubation media affects the protein corona composition [32], others report that only the quantity of protein changes and not the composition of the corona itself [33].

The optimal method to isolate LNPs from biological fluids is yet to be found, resulting in substantial variation in the methodology of protein corona isolation and identification in literature [34]. Choosing the correct isolation method is critical as it heavily affects protein corona composition [35,36]. Centrifugal isolation of LNPs is a relatively harsh method owing to the mechanical forces which may aggregate the LNPs and disrupt the protein corona. Moreover, specific isolation of LNPs via centrifugation is difficult by virtue of their inherent buoyancy, making this method prone to false positives due to co-isolation of naturally occurring nanoparticles such as extracellular vesicles, lipoproteins, protein complexes and -aggregates [7,35]. Size exclusion chromatography-based separation of LNPs, also used in the present study, is more delicate and allows accurate separation of nanoparticles and free protein. As the LNP peak in chromatograms is known to overlap with protein aggregates and extracellular vesicles [37], LNPs were fluorescently labeled to accurately identify LNP containing fractions (Fig. 3A).

Incorporation of biotin on the LNP surface allowed subsequent affinity-based separation of LNPs using streptavidin coated matrices, to further remove contaminants that were co-eluted during SEC isolation. Though the biotinylated PEG-decoration might alter the corona formation compared to the original Onpattro formulation, this effect was considered to be minor given the small molecular weight and neutral charge of biotin. Indeed, the uptake of LNPs in the biological fluids by HMEC and HCMEC was not affected by the decoration with biotin (Fig. S5). The biotinylated LNPs could be captured using streptavidin coated magnetic beads. By preceding this LNP capture with the SEC isolation, aspecific binding of free protein to the beads was limited, further increasing the accuracy of this method.

The protein fingerprints of CSF and plasma were visualized via protein gel electrophoresis followed by silver staining, which revealed an overall protein pattern overlap at most of the major protein bands. This was expected as CSF is a filtrate of plasma with 80% of its proteome originating from blood serum and about 20% of the proteins originating from the CNS [38,39]. Nevertheless, even with this basic technique, clear differences were observed between the biofluid protein fingerprints (Fig. S1).

Similar protein fingerprints emerge when comparing the protein bands from C-LNPs and P-LNPs. Also, one can note the large band around 15 kDa in both lanes, which is likely an artefact created by streptavidin monomers that are derived from the resin used to capture the LNPs. However, some fluid specific protein bands were visible at ~200 kDa, ~90 kDa and ~ 80 kDa for C-LNPs and 75 kDa and 12 kDa for P-LNPs, indicating unique corona components.

Enrichment of specific proteins on the LNPs was seen as certain bands, such as the one at 34 kDa, were prominent in the protein corona samples while they were not as visible in the biofluid dilutions. The 34 kDa band is likely to be ApoE, a known component of the Onpattro protein corona and crucial protein for LNP uptake by hepatocytes and tumor cell lines [9]. The ApoE band is more intense in the C-LNP

fingerprint suggesting a favorable corona is formed for cellular uptake in CSF. The relatively higher abundance of ApoE on C-LNPs was confirmed based on the ratio of fluorescence of labeled LNPs and immunostained ApoE. A higher abundance of ApoE was detected per LNP on C-LNPs than P-LNPs (Fig. 5C). Although absolute ApoE concentrations are much higher in human plasma than in CSF (50–70 μg/mL versus 3–10 μg/mL respectively), the relative ApoE concentration is higher in CSF (0.075% in plasma versus 1.08% in CSF) [40] which might explain the relative higher abundance of ApoE on C-LNPs.

The slightly higher molecular weight of this ApoE band on C-LNPs compared to on P-LNPs (Fig. 3B) can be explained by the compartmentalization of ApoE pools between the CNS and periphery. Brain derived ApoE is heavily glycosylated compared to peripheral ApoE [40] and would thus appear as a higher-weighted band than peripheral ApoE after gel electrophoresis.

Although definitive identification of the protein bands is not possible based on silver staining alone, the observed differences in protein fingerprints underline that distinct protein coronas are formed on C-LNPs compared to P-LNPs, which could affect LNP functionality (reviewed by 7, 14]. Moreover, it was hypothesized that cells would favorably interact with protein coronas from their own surroundings e.g., brain cells might interact better with C-LNPs, while peripheral cells might favor the protein corona found on P-LNPs. Therefore, brain endothelial (HCMEC) and brain tumor (U87) cells were compared with peripheral endothelial (HMEC) and tumor (MDA-MB-231) cells in terms of LNP uptake and processing to get insight into such tissue specific mechanisms.

A key event after Onpattro administration in vivo is the shedding of PEGylated lipids during circulation, to make room for proteins to attach to the particle surface and mediate LNP uptake by cells [9,41]. As this mechanism is time dependent [31,42], uptake was measured after 4 h, 24 h and 48 h to see whether the uptake changes over time between different fluids.

At 4 h, FCS consistently facilitated the highest uptake of LNPs in all cell types, followed by plasma and CSF. PBS always had the lowest uptake, most likely because of slowed down PEG-shedding kinetics from the LNPs due to a lack of opportunities to sufficiently desorb the PEG-lipids by proteins [31].

At 24 h, CSF conditions showed a significantly higher uptake of particles in both endothelial cell types compared to their respective plasma and FCS conditions and similar uptake to FCS in both tumor cell lines. This suggests that a more favorable protein corona for LNP uptake is formed with CSF proteins compared to plasma proteins. Even so, this favorable corona needs to develop over time. Indeed, at 48 h CSF protein coronas facilitated the highest uptake of LNPs in all cell types.

The hypothesized favorable interaction between brain cells C-LNPs was not observed as CSF consistently induced more LNP uptake from 24 h onwards, regardless of cell origin. No satisfying explanation was found for the lower MFIs at 48 h compared to 24 h for certain conditions. Whether this is due to intracellular degradation, excretion of RNA molecules [43,44] or reduced uptake of particles is not clear. An explanation is the observation that ApoE is replaced by other apolipoproteins on polymeric nanoparticles over time (>24 h), which would reduce cellular uptake of LNPs [45], yet this remains to be tested.

Next, the target knockdown efficacy of LNPs in different biological fluids was examined. The dual luciferase reporter system allows precise determination of siRNA mediated knockdown of firefly luciferase by using *Renilla* luciferase expression, which is unaffected by the siRNA, as internal control. The positive control with a commercial transfection agent shows that >50% knockdown could be achieved after 24 h and > 90% after 48 h with the cargo siRNA. Although the positive control achieves very similar knockdown between cells, LNPs show varying results in transfection efficiency. The endothelial cells were more susceptible to LNP mediated knockdown than the tumor cell lines. C-LNPs performed better than P-LNPs after 48 h in HMEC-*dluc* and HCMEC-*dluc*. Despite not showing the highest uptake, FCS LNPs induced the highest knockdown in both cell lines after 48 h.

MDA-MB-231-*dluc* were less susceptible to LNP mediated knockdown compared to the endothelial cells, with a maximal knockdown of <60% for LNPs and no apparent differences between the biological fluids at either time point. Even less knockdown was achieved in U87-*dluc* where no decrease of firefly expression over time and no differences between biofluids was observed. Low susceptibility of U87 to protein coronation of nanoparticles used for nucleic acid delivery has been described previously [46].

Here, it was shown that even for the same LNP, higher uptake in one biological fluid, does not directly translate into more efficient cargo delivery. Something that was also observed for different LNP formulations, where uptake was not a sufficient predictor of cargo delivery [47]. Although a threefold increased uptake of LNPs by HMEC was seen in CSF compared to in FCS, no significant difference in knockdown was observed. A similar observation was done for HCMEC and the tumor cell lines. This strongly suggests a protein corona mediated difference in cargo delivery efficiency.

LC-MS/MS was used to more specifically identify the proteins found on the LNP surface. Interestingly, brain specific proteins were only found in CSF containing samples indicating sample specificity and the enrichment of certain proteins was expected based on previous studies. For instance, both LNP containing samples showed an enrichment of apolipoproteins and immunoglobulins, some of which were not picked up in the controls due to the low abundance, indicating specific enrichment by the LNPs. The binding of immunoglobulins to a variety of nanoparticles, including lipid-based nanoparticles, has been shown previously [48]. The enrichment of apolipoproteins and other lipid binding proteins that was found in LNP containing fractions can be expected from the nature of the nanoparticles. ApoJ, ApoD and ApoE were most predominant in C-LNP fractions, while for P-LNPs we detected an enrichment of ApoC-III, ApoA-IV and ApoD (Fig. 9). Interestingly, ApoC-III, which was the most predominant apolipoprotein on P-LNPs (40.4% of total apolipoproteins), was absent in C-LNP fractions. This might be because ApoC-III is present in CSF in low concentrations (0.01% that of plasma) and is most likely dependent on plasma ApoA-I to reach the brain e.g., it is not or very little produced in brain tissues [49]. ApoC-III has been correlated with a lower uptake of nanoparticles [10,19]. The higher abundance of ApoC-III together with the relatively lower abundance of ApoE on P-LNPs as compared to C-LNPs might partly explain the lower cellular uptake of P-LNPs than C-LNPs. Remarkably, ApoJ has been shown to act as a stealth protein as it prevents IgGs from binding the nanoparticle surface [50], which in turn reduces the binding of complement system components such as immunoglobulins [48]. These observations are supported by the results here that show that the C-LNP corona contains a higher percentage of ApoJ than P-LNPs and indeed has fewer immunoglobulins found in the top 10 proteins based on relative abundance (2 for C-LNPs representing ~21% of the C-LNP corona compared to 7 for P-LNPs representing ~60% P-LNP corona) (Table S1). Given the limited number of replicates, this data can only be used as supportive information to speculate about certain observations. The discussed proteins were chosen based on their likely role in LNP-cell interactions due to the nature of these proteins (e.g., lipid processing and immune response). Nevertheless, the list of proteins found in the protein coronas is much larger and many proteins that have not been highlighted might be important players in LNP uptake and subsequent intracellular processing.

Besides the fact that the site of administration affects the LNP protein corona and with that, LNP performance, the health of the recipient is likely to play a role in the protein corona composition. Several studies have shown that, on a variety of nanoparticles, the composition of the protein corona depends on the health of the plasma donor (reviewed by [51]). In fact, the development of disease specific protein coronas has been used for disease and/or biomarker detection [52–55], indicating significant differences between coronas derived from healthy or diseased protein sources.

However, little is known about the in vivo implications of disease on

the development of protein coronas on LNPs specifically, and the consequences for their therapeutic efficacy remains to be investigated. Disease specific protein coronas have been identified on lipid based nanoparticles such as liposomes [56], which affected their biochemical properties [57] and ultimately their interaction with cells [58]. Interestingly, liposomes developed a protein corona in glioblastoma patient plasma that was distinctly different from their protein coronas developed in the plasma of healthy individuals [59]. Nonetheless, studies focusing on disease specific protein corona development on nucleic acid baring LNPs are lacking, especially in the context of the CNS. Recent results show that intrathecally administered DLin-MC3-DMA containing LNPs can deliver their cargo throughout the brain and can transfect all major brain tissue cell types in healthy mice [60,61]. Yet, it remains to be elucidated what role the protein corona plays in this aspect and how the distribution and transfection efficacy of LNPs would be affected by CNS pathologies. Proteomic characterization of CSF in patients with brain malignancies has revealed distinct proteomes in brain neoplasms [62] and other CNS pathologies such as dementia [63], multiple sclerosis [64] and Alzheimer's disease [65], suggesting that unique protein coronas will develop on nanoparticles exposed to CSF of these patients. This indicates that the proteome of the targeted condition needs to be considered during the development of LNP formulations.

5. Conclusion

In conclusion, our results indicate that intracranial delivery of Dlin-MC3-DMA LNPs results in the development of a protein corona which differs from that of intravenously administered particles, due to the acquisition of site-specific protein coronas. We show that the change in protein corona affects the cellular uptake kinetics of LNPs as well as their ability to effectively deliver cargo, while importantly, the increased uptake of LNPs does not guarantee more efficient target knockdown.

Funding

This publication is part of the project 15204 Technology for Oncology program which is financed by the Dutch Research Council (NWO) and Dutch Cancer Society (KWF).

CRediT authorship contribution statement

Demian van Straten: Writing – review & editing, Writing – original draft, Visualization, Methodology, Investigation, Conceptualization. **Helena Sork:** Writing – review & editing, Visualization, Investigation. **Luuk van de Schepop:** Investigation. **Rowan Frunt:** Investigation. **Kariem Ezzat:** Writing – review & editing. **Raymond M. Schiffelers:** Writing – review & editing, Supervision, Conceptualization.

Declaration of competing interest

KE cofounded REGAIN Therapeutics and is co-inventor of the patent "compositions and methods for treatment and/or prophylaxis of proteinopathies."

RMS is a part-time employee of Nanocell Therapeutics.

Data availability

Data will be made available on request.

Appendix A. Supplementary data

Supplementary data to this article can be found online at https://doi.org/10.1016/j.jconrel.2024.07.044.

References

[1] K.A. Whitehead, R. Langer, D.G. Anderson, Knocking down barriers: advances in siRNA delivery, Nat. Rev. Drug Discov. 8 (2) (2009) 129–138, https://doi.org/10.1038/nrd2742.
[2] J.A. Kulkarni, P.R. Cullis, R. van der Meel, Lipid nanoparticles enabling gene therapies: from concepts to clinical utility, Nucleic Acid Ther. 28 (3) (2018) 146–157, https://doi.org/10.1089/nat.2018.0721.
[3] J.A. Kulkarni, D. Witzigmann, S.B. Thomson, S. Chen, B.R. Leavitt, P.R. Cullis, R. van der Meel, The current landscape of nucleic acid therapeutics, Nat. Nanotechnol. 16 (6) (2021) 630–643, https://doi.org/10.1038/s41565-021-00898-0.
[4] D. Adams, A. Gonzalez-Duarte, W.D. O'Riordan, C.C. Yang, M. Ueda, A.V. Kristen, I. Tournev, H.H. Schmidt, T. Coelho, J.L. Berk, K.P. Lin, G. Vita, S. Attarian, V. Planté-Bordeneuve, M.M. Mezei, J.M. Campistol, J. Buades, T.H. Brannagan 3rd, B.J. Kim, J. Oh, O.B. Suhr, Patisiran, an RNAi therapeutic, for hereditary transthyretin amyloidosis, N. Engl. J. Med. 379 (1) (2018) 11–21, https://doi.org/10.1056/NEJMoa1716153.
[5] X. Zhang, V. Goel, H. Attarwala, M.T. Sweetser, V.A. Clausen, G.J. Robbie, Patisiran pharmacokinetics, pharmacodynamics, and exposure-response analyses in the phase 3 APOLLO trial in patients with hereditary transthyretin-mediated (hATTR) amyloidosis, J. Clin. Pharmacol. 60 (1) (2020) 37–49, https://doi.org/10.1002/jcph.1480.
[6] M.P. Monopoli, C. Aberg, A. Salvati, K.A. Dawson, Biomolecular coronas provide the biological identity of nanosized materials, Nat. Nanotechnol. 7 (12) (2012) 779–786, https://doi.org/10.1038/nnano.2012.207.
[7] V. Francia, R.M. Schiffelers, P.R. Cullis, D. Witzigmann, The biomolecular Corona of lipid nanoparticles for gene therapy, Bioconjug. Chem. 31 (9) (2020) 2046–2059, https://doi.org/10.1021/acs.bioconjchem.0c00366.
[8] S.A. Dilliard, Q. Cheng, D.J. Siegwart, On the mechanism of tissue-specific mRNA delivery by selective organ targeting nanoparticles, Proc. Natl. Acad. Sci. USA 118 (52) (2021) e2109256118, https://doi.org/10.1073/pnas.2109256118.
[9] A. Akinc, W. Querbes, S. De, J. Qin, M. Frank-Kamenetsky, K.N. Jayaprakash, M. Jayaraman, K.G. Rajeev, W.L. Cantley, J.R. Dorkin, J.S. Butler, L. Qin, T. Racie, A. Sprague, E. Fava, A. Zeigerer, M.J. Hope, M. Zerial, D.W. Sah, K. Fitzgerald, M. A. Maier, Targeted delivery of RNAi therapeutics with endogenous and exogenous ligand-based mechanisms, Mol. Therapy: J. American Soci. Gene Therapy 18 (7) (2010) 1357–1364, https://doi.org/10.1038/mt.2010.85.
[10] D. Chen, S. Ganesh, W. Wang, M. Amiji, The role of surface chemistry in serum protein corona-mediated cellular delivery and gene silencing with lipid nanoparticles, Nanoscale 11 (18) (2019) 8760–8775, https://doi.org/10.1039/c8nr09855g.
[11] H. Mohammad-Beigi, Y. Hayashi, C.M. Zeuthen, H. Eskandari, C. Scavenius, K. Juul-Madsen, T. Vorup-Jensen, J.J. Enghild, D.S. Sutherland, Mapping and identification of soft corona proteins at nanoparticles and their impact on cellular association, Nat. Commun. 11 (1) (2020) 4535, https://doi.org/10.1038/s41467-020-18237-7.
[12] M. Wang, O.J.R. Gustafsson, E.H. Pilkington, A. Kakinen, I. Javed, A. Faridi, T. P. Davis, P.C. Ke, Nanoparticle-proteome in vitro and in vivo, J. Mater. Chem. B 6 (38) (2018) 6026–6041, https://doi.org/10.1039/c8tb01634h.
[13] M. Falahati, F. Attar, M. Sharifi, T. Haertlé, J.F. Berret, R.H. Khan, A.A. Saboury, A health concern regarding the protein corona, aggregation and disaggregation, Biochim. Biophys. Acta, Gen. Subj. 1863 (5) (2019) 971–991, https://doi.org/10.1016/j.bbagen.2019.02.012.
[14] V. Francia, D. Montizaan, A. Salvati, Interactions at the cell membrane and pathways of internalization of nano-sized materials for nanomedicine, Beilstein J. Nanotechnol. 11 (2020) 338–353, https://doi.org/10.3762/bjnano.11.25.
[15] M. Mahmoudi, M.P. Landry, A. Moore, R. Coreas, The protein corona from nanomedicine to environmental science, Nat. Rev. Mater. (2023) 1–17. Advance online publication. https://doi.org/10.1038/s41578-023-00552-2.
[16] F. Sebastiani, M. Yanez Arteta, M. Lerche, L. Porcar, C. Lang, R.A. Bragg, C. S. Elmore, V.R. Krishnamurthy, R.A. Russell, T. Darwish, H. Pichler, S. Waldie, M. Moulin, M. Haertlein, V.T. Forsyth, L. Lindfors, M. Cárdenas, Apolipoprotein E binding drives structural and compositional rearrangement of mRNA-containing lipid nanoparticles, ACS Nano 15 (4) (2021) 6709–6722, https://doi.org/10.1021/acsnano.0c10064.
[17] Q. Cheng, T. Wei, L. Farbiak, L.T. Johnson, S.A. Dilliard, D.J. Siegwart, Selective organ targeting (SORT) nanoparticles for tissue-specific mRNA delivery and CRISPR-Cas gene editing, Nat. Nanotechnol. 15 (4) (2020) 313–320, https://doi.org/10.1038/s41565-020-0669-6.
[18] R. Zhang, R. El-Mayta, T.J. Murdoch, C.C. Warzecha, M.M. Billingsley, S. J. Shepherd, N. Gong, L. Wang, J.M. Wilson, D. Lee, M.J. Mitchell, Helper lipid structure influences protein adsorption and delivery of lipid nanoparticles to spleen and liver, Biomater. Sci. 9 (4) (2021) 1449–1463, https://doi.org/10.1039/d0bm01609h.
[19] S. Ritz, S. Schöttler, N. Kotman, G. Baier, A. Musyanovych, J. Kuharev, K. Landfester, H. Schild, O. Jahn, S. Tenzer, V. Mailänder, Protein corona of nanoparticles: distinct proteins regulate the cellular uptake, Biomacromolecules 16 (4) (2015) 1311–1321, https://doi.org/10.1021/acs.biomac.5b00108.
[20] J. Martel, D. Young, A. Young, C.Y. Wu, C.D. Chen, J.S. Yu, J.D. Young, Comprehensive proteomic analysis of mineral nanoparticles derived from human body fluids and analyzed by liquid chromatography-tandem mass spectrometry, Anal. Biochem. 418 (1) (2011) 111–125, https://doi.org/10.1016/j.ab.2011.06.018.
[21] M. Lundqvist, C. Augustsson, M. Lilja, K. Lundkvist, B. Dahlbäck, S. Linse, T. Cedervall, The nanoparticle protein corona formed in human blood or human

blood fractions, PLoS One 12 (4) (2017) e0175871, https://doi.org/10.1371/journal.pone.0175871.
[22] R.L. Pinals, D. Yang, D.J. Rosenberg, T. Chaudhary, A.R. Crothers, A.T. Iavarone, M. Hammel, M.P. Landry, Quantitative protein Corona composition and dynamics on carbon nanotubes in biological environments, Angew. Chem. Int. Ed. Eng. 59 (52) (2020) 23668–23677, https://doi.org/10.1002/anie.202008175.
[23] S. Ingusci, G. Verlengia, M. Soukupova, S. Zucchini, M. Simonato, Gene therapy tools for brain diseases, Front. Pharmacol. 10 (2019) 724, https://doi.org/10.3389/fphar.2019.00724.
[24] T.R. Flotte, D.J. Gessler, Gene therapy for rare neurological disorders, Clin. Pharmacol. Ther. 111 (4) (2022) 743–757, https://doi.org/10.1002/cpt.2543.
[25] M. Simonato, J. Bennett, N.M. Boulis, M.G. Castro, D.J. Fink, W.F. Goins, S.J. Gray, P.R. Lowenstein, L.H. Vandenberghe, T.J. Wilson, J.H. Wolfe, J.C. Glorioso, Progress in gene therapy for neurological disorders, Nat. Rev. Neurol. 9 (5) (2013) 277–291, https://doi.org/10.1038/nrneurol.2013.56.
[26] A. Cox, P. Andreozzi, R. Dal Magro, F. Fiordaliso, A. Corbelli, L. Talamini, C. Chinello, F. Raimondo, F. Magni, M. Tringali, S. Krol, P. Jacob Silva, F. Stellacci, M. Masserini, F. Re, Evolution of nanoparticle protein Corona across the blood-brain barrier, ACS Nano 12 (7) (2018) 7292–7300, https://doi.org/10.1021/acsnano.8b03500.
[27] M.J.W. Evers, S.I. van de Wakker, E.M. de Groot, O.G. de Jong, J.J.J. Gitz-François, C.S. Seinen, J.P.G. Sluijter, R.M. Schiffelers, P. Vader, Functional siRNA delivery by extracellular vesicle-liposome hybrid nanoparticles, Adv. Healthc. Mater. 11 (5) (2022) e2101202, https://doi.org/10.1002/adhm.202101202.
[28] D.E. Murphy, O.G. de Jong, M.J.W. Evers, M. Nurazizah, R.M. Schiffelers, P. Vader, Natural or synthetic RNA delivery: a stoichiometric comparison of extracellular vesicles and synthetic nanoparticles, Nano Lett. 21 (4) (2021) 1888–1895, https://doi.org/10.1021/acs.nanolett.1c00094.
[29] A.C. Anselmo, S. Mitragotri, Nanoparticles in the clinic: an update, Bioeng. & Translat. Med. 4 (3) (2019) e10143, https://doi.org/10.1002/btm2.10143.
[30] E. Jankovska, M. Svitek, K. Holada, J. Petrak, Affinity depletion versus relative protein enrichment: a side-by-side comparison of two major strategies for increasing human cerebrospinal fluid proteome coverage, Clin. Proteomics 16 (2019) 9, https://doi.org/10.1186/s12014-019-9229-1.
[31] A. Gallud, M.J. Munson, K. Liu, A. Idström, H.M.G. Barriga, S.R. Tabaei, N. Aliakbarinodehi, M. Ojansivu, Q. Lubart, J.J. Doutch, M.N. Holme, L. Evenäs, L. Lindfors, M.M. Stevens, A. Collén, A. Sabirsh, F. Höök, E.K. Esbjörner, Time evolution of PEG-shedding and serum protein coronation determines the cell uptake kinetics and delivery of lipid nanoparticle formulated mRNA, bioRxiv (2021), https://doi.org/10.1101/2021.08.20.457104, 2021.08.20.457104.
[32] V. Francia, K. Yang, S. Deville, C. Reker-Smit, I. Nelissen, A. Salvati, Corona composition can affect the mechanisms cells use to internalize nanoparticles, ACS Nano 13 (10) (2019) 11107–11121, https://doi.org/10.1021/acsnano.9b03824.
[33] K. Partikel, R. Korte, D. Mulac, H.U. Humpf, K. Langer, Serum type and concentration both affect the protein-corona composition of PLGA nanoparticles, Beilstein J. Nanotechnol. 10 (2019) 1002–1015, https://doi.org/10.3762/bjnano.10.101.
[34] L. Böhmert, L. Voß, V. Stock, A. Braeuning, A. Lampena, H. Sieg, Isolation methods for particle protein corona complexes from protein-rich matrices, Nanoscale Adv. 2 (2020) 563–582, https://doi.org/10.1039/C9NA00537D.
[35] R. Pattipeiluhu, S. Crielaard, I. Klein-Schiphorst, B.I. Florea, A. Kros, F. Campbell, Unbiased identification of the liposome protein Corona using Photoaffinity-based Chemoproteomics, ACS Cent. Sci. 6 (4) (2020) 535–545, https://doi.org/10.1021/acscentsci.9b01222.
[36] K. Hoang, K.E. Wheeler, C.J. Murphy, Isolation methods influence the protein Corona composition on gold-coated Iron oxide nanoparticles, Anal. Chem. 94 (11) (2022) 4737–4746, https://doi.org/10.1021/acs.analchem.1c05243.
[37] P.M. Vanderboom, S. Dasari, G.N. Ruegsegger, M.W. Pataky, F. Lucien, C. J. Heppelmann, I.R. Lanza, K.S. Nair, A size-exclusion-based approach for purifying extracellular vesicles from human plasma, Cell Report. Meth. 1 (3) (2021) 100055, https://doi.org/10.1016/j.crmeth.2021.100055.
[38] A. Regeniter, J. Kuhle, M. Mehling, H. Möller, U. Wurster, H. Freidank, W.H. Siede, A modern approach to CSF analysis: pathophysiology, clinical application, proof of concept and laboratory reporting, Clin. Neurol. Eurosurg. 111 (4) (2009) 313–318, https://doi.org/10.1016/j.clineuro.2008.12.004.
[39] A.C. Kroksveen, J.A. Opsahl, T.T. Aye, R.J. Ulvik, F.S. Berven, Proteomics of human cerebrospinal fluid: discovery and verification of biomarker candidates in neurodegenerative diseases using quantitative proteomics, J. Proteome 74 (4) (2011) 371–388, https://doi.org/10.1016/j.jprot.2010.11.010.
[40] D. Chernick, S. Ortiz-Valle, A. Jeong, W. Qu, L. Li, Peripheral versus central nervous system APOE in Alzheimer's disease: interplay across the blood-brain barrier, Neurosci. Lett. 708 (2019) 134306, https://doi.org/10.1016/j.neulet.2019.134306.
[41] B.L. Mui, Y.K. Tam, M. Jayaraman, S.M. Ansell, X. Du, Y.Y. Tam, P.J. Lin, S. Chen, J.K. Narayanannair, K.G. Rajeev, M. Manoharan, A. Akinc, M.A. Maier, P. Cullis, T. D. Madden, M.J. Hope, Influence of polyethylene glycol lipid desorption rates on pharmacokinetics and pharmacodynamics of siRNA lipid nanoparticles. Molecular therapy, Nucleic Acids 2 (12) (2013) e139, https://doi.org/10.1038/mtna.2013.66.
[42] X. Zhu, W. Tao, D. Liu, J. Wu, Z. Guo, X. Ji, Z. Bharwani, L. Zhao, X. Zhao, O. C. Farokhzad, J. Shi, Surface De-PEGylation controls nanoparticle-mediated siRNA delivery *in vitro* and *in vivo*, Theranostics 7 (7) (2017) 1990–2002, https://doi.org/10.7150/thno.18136.
[43] G. Sahay, W. Querbes, C. Alabi, A. Eltoukhy, S. Sarkar, C. Zurenko, E. Karagiannis, K. Love, D. Chen, R. Zoncu, Y. Buganim, A. Schroeder, R. Langer, D.G. Anderson, Efficiency of siRNA delivery by lipid nanoparticles is limited by endocytic recycling, Nat. Biotechnol. 31 (7) (2013) 653–658, https://doi.org/10.1038/nbt.2614.
[44] M. Maugeri, M. Nawaz, A. Papadimitriou, A. Angerfors, A. Camponeschi, M. Na, M. Hölttä, P. Skantze, S. Johansson, M. Sundqvist, J. Lindquist, T. Kjellman, I. L. Mårtensson, T. Jin, P. Sunnerhagen, S. Östman, L. Lindfors, H. Valadi, Linkage between endosomal escape of LNP-mRNA and loading into EVs for transport to other cells, Nat. Commun. 10 (1) (2019) 4333, https://doi.org/10.1038/s41467-019-12275-6.
[45] T. Lima, K. Bernfur, M. Vilanova, T. Cedervall, Understanding the lipid and protein Corona formation on different sized polymeric nanoparticles, Sci. Rep. 10 (1) (2020) 1129, https://doi.org/10.1038/s41598-020-57943-6.
[46] E. Quagliarini, R. Di Santo, S. Palchetti, G. Ferri, F. Cardarelli, D. Pozzi, G. Caracciolo, Effect of protein Corona on the transfection efficiency of lipid-coated graphene oxide-based cell transfection reagents, Pharmaceutics 12 (2) (2020) 113, https://doi.org/10.3390/pharmaceutics12020113.
[47] P. Paramasivam, C. Franke, M. Stöter, A. Höijer, S. Bartesaghi, A. Sabirsh, L. Lindfors, M.Y. Arteta, A. Dahlén, A. Bak, S. Andersson, Y. Kalaidzidis, M. Bickle, M. Zerial, Endosomal escape of delivered mRNA from endosomal recycling tubules visualized at the nanoscale, J. Cell Biol. 221 (2) (2022) e202110137, https://doi.org/10.1083/jcb.202110137.
[48] V.P. Vu, G.B. Gifford, F. Chen, H. Benasutti, G. Wang, E.V. Groman, R. Scheinman, L. Saba, S.M. Moghimi, D. Simberg, Immunoglobulin deposition on biomolecule corona determines complement opsonization efficiency of preclinical and clinical nanoparticles, Nat. Nanotechnol. 14 (3) (2019) 260–268, https://doi.org/10.1038/s41565-018-0344-3.
[49] M. Koch, J.D. Furtado, K. Falk, F. Leypoldt, K.J. Mukamal, M.K. Jensen, Apolipoproteins and their subspecies in human cerebrospinal fluid and plasma, Alzheimer's & Dementia (Amsterdam, Netherlands) 6 (2017) 182–187, https://doi.org/10.1016/j.dadm.2017.01.007.
[50] D. Prozeller, J. Pereira, J. Simon, V. Mailänder, S. Morsbach, K. Landfester, Prevention of Dominant IgG Adsorption on Nanocarriers in IgG-Enriched Blood Plasma by Clusterin Precoating, Adv. Sci. (Weinheim, Baden-Wurttemberg, Germany) vol. 6 (10) (2019) 1802199, https://doi.org/10.1002/advs.201802199.
[51] M. García Vence, M.D.P. Chantada-Vázquez, S. Vázquez-Estévez, J. Manuel Cameselle-Teijeiro, S.B. Bravo, C. Núñez, Potential clinical applications of the personalized, disease-specific protein corona on nanoparticles, Clini. Chim. Acta; Int. J. Clin. Chem. 501 (2020) 102–111, https://doi.org/10.1016/j.cca.2019.10.027.
[52] D. Caputo, M. Papi, R. Coppola, S. Palchetti, L. Digiacomo, G. Caracciolo, D. Pozzi, A protein corona-enabled blood test for early cancer detection, Nanoscale 9 (1) (2017) 349–354, https://doi.org/10.1039/c6nr05609a.
[53] S. Palchetti, D. Caputo, L. Digiacomo, A.L. Capriotti, R. Coppola, D. Pozzi, G. Caracciolo, Protein Corona fingerprints of liposomes: new opportunities for targeted drug delivery and early detection in pancreatic Cancer, Pharmaceutics 11 (1) (2019) 31, https://doi.org/10.3390/pharmaceutics11010031.
[54] J.E. Blume, W.C. Manning, G. Troiano, D. Hornburg, M. Figa, L. Hesterberg, T. L. Platt, X. Zhao, R.A. Cuaresma, P.A. Everley, M. Ko, H. Liou, M. Mahoney, S. Ferdosi, E.M. Elgierari, C. Stolarczyk, B. Tangeysh, H. Xia, R. Benz, A. Siddiqui, O.C. Farokhzad, Rapid, deep and precise profiling of the plasma proteome with multi-nanoparticle protein corona, Nat. Commun. 11 (1) (2020) 3662, https://doi.org/10.1038/s41467-020-17033-7.
[55] L. Digiacomo, K. Jafari-Khouzani, S. Palchetti, D. Pozzi, A.L. Capriotti, A. Laganà, R. Zenezini Chiozzi, D. Caputo, C. Cascone, R. Coppola, G. Flammia, V. Altomare, A. Grasso, M. Mahmoudi, G. Caracciolo, A protein corona sensor array detects breast and prostate cancers, Nanoscale 12 (32) (2020) 16697–16704, https://doi.org/10.1039/d0nr03439h.
[56] V. Colapicchioni, M. Tilio, L. Digiacomo, V. Gambini, S. Palchetti, C. Marchini, D. Pozzi, S. Occhipinti, A. Amici, G. Caracciolo, Personalized liposome-protein corona in the blood of breast, gastric and pancreatic cancer patients, Int. J. Biochem. Cell Biol. 75 (2016) 180–187, https://doi.org/10.1016/j.biocel.2015.09.002.
[57] G. Caracciolo, D. Caputo, D. Pozzi, V. Colapicchioni, R. Coppola, Size and charge of nanoparticles following incubation with human plasma of healthy and pancreatic cancer patients, Colloids Surf. B: Biointerfaces 123 (2014) 673–678, https://doi.org/10.1016/j.colsurfb.2014.10.008.
[58] Y. Ju, H.G. Kelly, L.F. Dagley, A. Reynaldi, T.E. Schlub, S.K. Spall, C.A. Bell, J. Cui, A.J. Mitchell, Z. Lin, A.K. Wheatley, K.J. Thurecht, M.P. Davenport, A.I. Webb, F. Caruso, S.J. Kent, Person-specific biomolecular coronas modulate nanoparticle interactions with immune cells in human blood, ACS Nano 14 (11) (2020) 15723–15737, https://doi.org/10.1021/acsnano.0c06679.
[59] G. Caracciolo, R. Safavi-Sohi, R. Malekzadeh, H. Poustchi, M. Vasighi, R. Zenezini Chiozzi, A.L. Capriotti, A. Laganà, M. Hajipour, M. Di Domenico, A. Di Carlo, D. Caputo, H. Aghaverdi, M. Papi, V. Palmieri, A. Santoni, S. Palchetti, L. Digiacomo, D. Pozzi, K.S. Suslick, M. Mahmoudi, Disease-specific protein corona sensor arrays may have disease detection capacity, Nanoscale Horiz. 4 (2019) 1063–1076, https://doi.org/10.1039/C9NH00097F.
[60] J. Tuma, Y.J. Chen, M.G. Collins, A. Paul, J. Li, H. Han, R. Sharma, N. Murthy, H. Y. Lee, Lipid nanoparticles deliver mRNA to the brain after an intracerebral injection, Biochemistry 62 (24) (2023) 3533–3547, https://doi.org/10.1021/acs.biochem.3c00371.
[61] A.E. Byrnes, S.L. Dominguez, C.W. Yen, B.I. Laufer, O. Foreman, M. Reichelt, H. Lin, M. Sagolla, K. Hötzel, H. Ngu, C. Soendergaard, A. Estevez, H.C. Lin, A. Goyon, J. Bian, J. Lin, F.I. Hinz, B.A. Friedman, A. Easton, C.C. Hoogenraad, Lipid nanoparticle delivery limits antisense oligonucleotide activity and cellular distribution in the brain after intracerebroventricular injection, Mol. Therap.: Nucleic Acids 32 (2023) 773–793, https://doi.org/10.1016/j.omtn.2023.05.005.

[62] D. Schmid, U. Warnken, P. Latzer, D.C. Hoffmann, J. Roth, S. Kutschmann, H. Jaschonek, P. Rübmann, M. Foltyn, P. Vollmuth, F. Winkler, C. Seliger, M. Felix, F. Sahm, J. Haas, D. Reuss, M. Bendszus, B. Wildemann, A. von Deimling, W. Wick, T. Kessler, Diagnostic biomarkers from proteomic characterization of cerebrospinal fluid in patients with brain malignancies, J. Neurochem. 158 (2) (2021) 522–538, https://doi.org/10.1111/jnc.15350.

[63] A. Ishiki, M. Kamada, Y. Kawamura, C. Terao, F. Shimoda, N. Tomita, H. Arai, K. Furukawa, Glial fibrillar acidic protein in the cerebrospinal fluid of Alzheimer's disease, dementia with Lewy bodies, and frontotemporal lobar degeneration, J. Neurochem. 136 (2) (2016) 258–261, https://doi.org/10.1111/jnc.13399.

[64] M.P. Stoop, T.F. Runia, C. Stingl, R.M. van der Vuurst de Vries, T.M. Luider, R. Q. Hintzen, Decreased neuro-axonal proteins in CSF at first attack of suspected multiple sclerosis, Proteomics Clin. Appl. 11 (11−12) (2017), https://doi.org/10.1002/prca.201700005.

[65] B.M. Tijms, E.M. Vromen, O. Mjaavatten, H. Holstege, L.M. Reus, S. van der Lee, K. E.J. Wesenhagen, L. Lorenzini, L. Vermunt, V. Venkatraghavan, N. Tesi, J. Tomassen, A. den Braber, J. Goossens, E. Vanmechelen, F. Barkhof, Y.A. L. Pijnenburg, W.M. van der Flier, C.E. Teunissen, F.S. Berven, P.J. Visser, Cerebrospinal fluid proteomics in patients with Alzheimer's disease reveals five molecular subtypes with distinct genetic risk profiles, Nature Aging 4 (1) (2024) 33–47, https://doi.org/10.1038/s43587-023-00550-7.